PERGAMON

Journal of Structural Geology 24 (2002) 1157–1170

JOURNAL OF STRUCTURAL GEOLOGY

www.elsevier.com/locate/jstrugeo

Structural evolution of a quartz–sillimanite vein and nodule complex in a late-to post-tectonic leucogranite, Western Adirondack Highlands, New York

James McLelland[a,*], Arthur Goldstein[a], Betsy Cunningham[a], Christopher Olson[a], Suzanne Orrell[b]

[a]*Department of Geology, Colgate University, Hamilton, NY 13346, USA*
[b]*Department of Geology, Hobart and William Smith College, Geneva, NY 14456, USA*

Received 22 November 2000; revised 5 April 2001; accepted 10 May 2001

Abstract

Quartz–sillimanite veins and nodules within the carapace of a late- to post- tectonic leucogranite crosscut one another as well as calcsilicate schlieren. These relationships document a fracture-related and hydrothermal origin of the vein and nodule complex. Two dominant orientations (N50E, N20E) are observed with the former being the oldest and most deformed. Both of these sets have undergone deformation, including boudinage of veins to produce nodules. Zircon geochronology fixes the emplacement age of the leucogranite at 1035.1 ± 3.8 Ma and late crosscutting pegmatites at 1034 ± 10 Ma, hence the vein–nodule complex must fall within this interval. Late dikes of leucogranite truncate the complex and document the continued presence of magma during vein–nodule formation. Anisotropy of magnetic susceptibility (AMS) in the leucogranite carapace reveals an approximately horizontal flow direction, within a plane striking N49E and dipping moderately to the northwest. In this regime, quartz–sillimanite veins formed initially as tension fractures in subvertical NNE orientations either as a result of high fluid pressures or rapid sinistral shear along the N50E contact. Progressive sinistral shear rotated the veins counterclockwise causing buckling followed by boudinage and rotation of fragments into near parallelism with the N50E contact. Strain was accommodated by slip between crystals and melt migration with an estimated melt fraction of at least 30%. Multiple episodes of fracturing and vein formation appear to have occurred. Final deformation of the carapace and the vein–nodule complex is envisioned as a flattening against the contact, perhaps as a result of pluton inflation. Melt was still present after this event as evidenced by post-vein granite and pegmatite dikes, commonly with sinistral shear along the dike margin.

Keywords: Quartz–sillimanite; Carapace; Leucogranite

1. Introduction

Quartz–sillimanite nodules and segregations have received considerable attention in the literature and diverse origins have been proposed (Losert, 1968; Vernon, 1979; Kerrick, 1988; Markl and Schumacher, 1996; Nabeleck, 1997), but their genesis remains somewhat enigmatic. Within the Adirondack Mountains (Fig. 1) vein-like and nodular segregations consisting of quartz and sillimanite occur locally within several rock types but are best developed in alaskitic leucogranites representative of late-to post-tectonic Lyon Mt. granitic gneiss (LMG) (Postel, 1952; Buddington and Leonard, 1962; McLelland et al., 1996). An exceptionally well-exposed example of quartz–sillimanite veins and nodules occurs in the bed of the Moose River near the hamlet of Lyonsdale Falls in the west-central Adirondack Highlands (Fig. 2). Here semi-continuous, water-washed exposures of leucogranite, compositionally similar to high-silica LMG, extend downstream for over 3 km and contain extraordinary examples of quartz–sillimanite veins and nodules. Intermediate forms and structural relationships indicate that the nodules originated by disruption of veins by boudinage and/or magmatic displacement leading to disharmonic configurations. Recently, McLelland et al. (2002) have reported on the geochemistry of these, and related, features in the Adirondack Highlands, and have concluded that the quartz–sillimanite veins and nodules are the result of alteration and base-cation leaching by high temperature (550–650°C) hydrothermal fluids of dominantly magmatic origin. This mechanism is similar to that proposed by

* Corresponding author. Tel.: +1-518-835-8561; fax: +1-315-228-7187.
E-mail address: jmclelland@mail.colgate.edu (J. McLelland).

0191-8141/02/$ - see front matter
PII: S0191-8141(01)00098-0

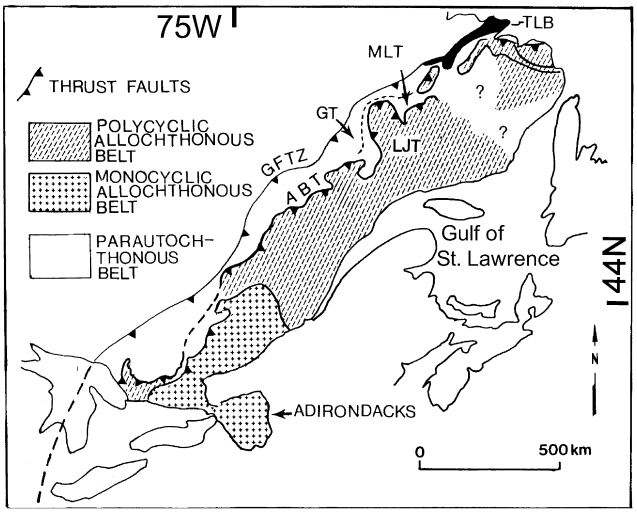

Fig. 1. Generalized location map of the Adirondack Mts. as a southwestern extension of the Grenville Province of Canada. The three major tectonic divisions of Rivers (1997) are identified in the legend. ABT — Allochthonous Boundary Thrust; GFTZ — Grenville Front Tectonic Zone; GT — Gagnon Terrane; LJT — Lac Joseph Terrane; MLT — Melville Lake Terrane; TLB — Trans-Labrador batholith.

Vernon (1979) for distinctive quartz–sillimanite occurrences in high-grade gneisses of the Cooma Complex, Australia. Zircon geochronology indicates that formation of the vein–nodule complex took place during the waning stages of the ca. 1090–1030 Ma Ottawan Orogeny (McLelland et al., 2001a).

The purpose of this paper is to investigate the structural and textural nature of the veins, nodules, and their host rock and to propose a coherent structural model for the origin of the quartz–sillimanite vein–nodule complex at Lyonsdale Falls, New York. Zircon geochronology bearing on the emplacement age of the granite is also presented and serves to constrain formation of the vein–nodule complex to the interval of magma crystallization.

2. Description of quartz–sillimanite vein–nodule complex

The vein–nodule complex near Lyonsdale is situated in a portion of the host leucogranite that lies near its contact with country rock metasediments (dominantly calcsilicate) and older granitoids of the Adirondack anorthosite–mangerite–charnockite–granite (AMCG) suite. The contact, which strikes approximately N50E, is locally exposed along strike approximately 0.25 mile upstream from Lyonsdale and is crosscut by dikes of granite and pegmatite extending from the leucogranite. Based on these observations, the Lyonsdale exposures are interpreted as lying within the carapace of the leucogranite pluton, and the features described below should be considered in that context. There is insufficient exposure of country rock to establish whether it contains structures like those in the leucogranite. The depth of emplacement of the leucogranite remains highly uncertain, but McLelland et al. (2002) present arguments for depths not exceeding 10–12 km. Included in these are the hypersolvus nature of the leucogranite despite its apparently hydrous nature and the fact that it plots at low pressures in the normative haplogranite system (SiO_2–Ab–Or).

Fig. 3 shows a typical exposure of quartz–sillimanite veins and nodules developed within leucogranite at

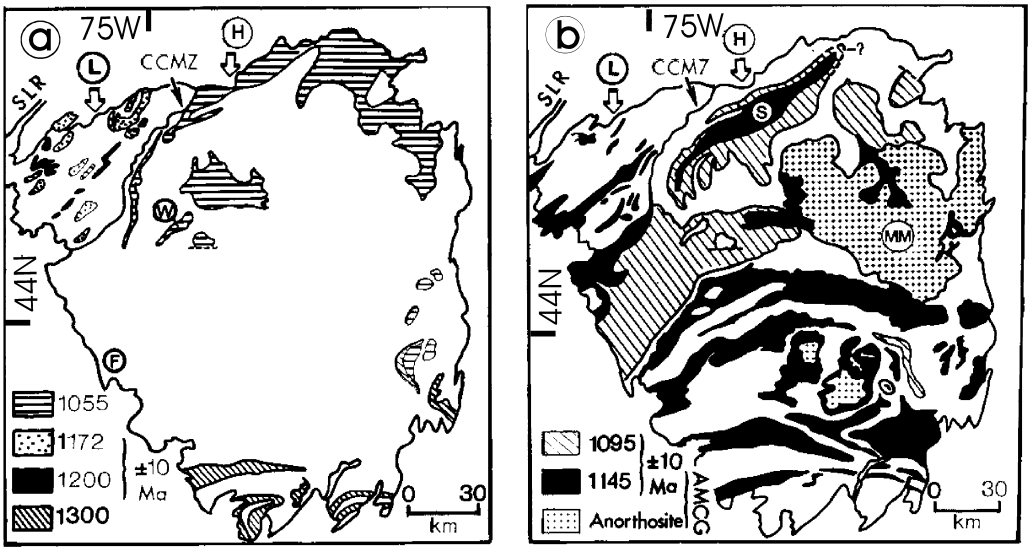

Fig. 2. Generalized geological/chronological map of the Adirondack Mts., New York divided into panels (a) and (b) for clarity. The study area at Lyonsdale Falls is designated by F on panel (a). The Lyon Mt. granitic gneiss (LMG) discussed in the text corresponds to the ca. 1055 Ma unit designated by horizontal ruling in panel (a). Other units are: 1300 Ma — tonalitic suite; 1200 Ma — Antwerp granitoids; 1172 Ma — Hyde School Gneiss; 1145 Ma — anorthosite–mangerite–charnockite–granite (AMCG) suite; 1095 Ma — Hawkeye granite suite; MM — Marcy anorthosite massif; S — Stark Anticline; W — Wanakena; H — Highlands; L — Lowlands; CCMZ — Carthage–Colton Mylonite Zone; SLR — St. Lawrence River.

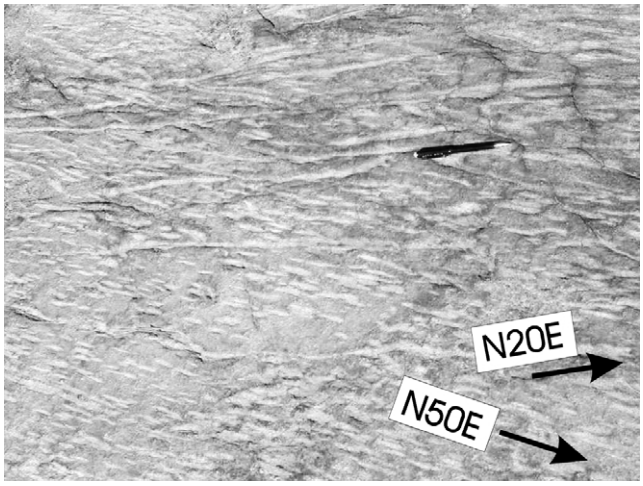

Fig. 3. Representative exposure of quartz–sillimanite vein–nodule complex in the Moose River bed at Lyonsdale Falls. Small N50E (see arrows) nodules are crosscut by continuous and semi-continuous N20E veins (see arrows). Note the disruption by boudinage along strike of many of the N20E veins and the manner in which most N50E nodules form aligned trains indicating that they also represent disrupted veins. Pencil = 15 cm.

Lyonsdale Falls, New York. Two principal directions (averaging N20E ± 10° and N50E ± 10°) are present and are dominant in the vein–nodule complex. Both sets dip approximately 40–60°NW, but the two-dimensional surfaces of the exposures make it difficult to obtain extensive dip data. Typically, the N50E set occurs as small elliptical nodules that have undergone ductile deformation, whereas the N30E set more commonly occurs as continuous or boudinaged veins and blocky nodules. Crosscutting relationships exist between these sets (Fig. 3) where the older, N50E veins have been boudinaged into nodule trains and are transected by still largely intact N20E veins. Similarly, in Fig. 4 a N30E vein crosscuts elliptical nodules typical of the N50E set. Blocky nodules and veinlets of the

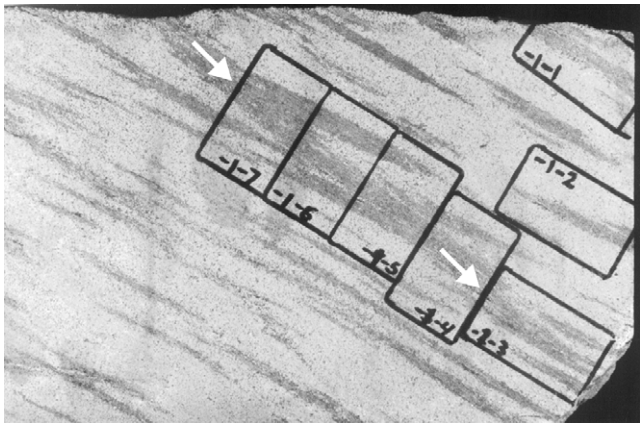

Fig. 4. Polished slab of quartz–sillimanite veins and nodules in host leucogranite. A later N30E vein (within the row of five thin section outlines at center of photo and indicated by arrows) crosscuts N50E nodules thus demonstrating sequential formation of these features. Rectangles (27×46 mm^2) mark thin section locations.

N20E set are shown in Fig. 5a and b, where they demonstrably crosscut dark, calcsilicate schleiren in the host leucogranite. Some of the veinlets are associated with en échelon sinistral shear fractures that displace the schleiren (Fig. 5b). Despite their high degree of disruption by boudinage, it is possible to occasionally find examples of the early N50E nodules that preserve crosscutting relationships. These observations establish that both sets of quartz–sillimanite veins and nodules postdate emplacement of the leucogranite and are closely related to fracturing of this host rock. Accordingly, they cannot be explained as the result of xenolithic material, e.g. clay, incorporated into the leucogranite and altered by it.

It is common for both sets of nodules to be aligned in trains (Figs. 3 and 5a). This relationship indicates that the nodules represent veins disrupted by boudinage. Locally, the nodules form en échelon arrays centered on calc–silicate schleiren, suggesting a shear zone origin (Fig. 5b). Boudinage-type vein disruption is clearly evident upon close inspection of Fig. 3, and some of the blocky nodules in Fig. 5a appear to fit back together along a disrupted N20E vein trend. Similar disruption of a vein (Fig. 6) has given rise to a N50E trending nodule train. Note that a crosscutting N20E vein has *not* been disrupted and emphasizes the time sequence of vein and nodule formation. Although it is not common, vein disruption can be associated with folding such as that shown in Fig. 7 where several fragments of the N20E vein set occur as disrupted and disharmonic folds.

The sequence of vein–nodule events is further borne out by quartz–sillimanite veins that wander across outcrop surfaces marked by pronounced nodular disruption without showing similar effects themselves (Fig. 8). Clearly, these veins must have formed late in the sequence and experienced only mild deformation, which resulted in open folding and nascent disruption. Even more striking is the existence of late NW-trending dikes and sheets of nodule-free leucogranite that crosscut the nodule- and vein-bearing host leucogranite (Fig. 9). These dikes and sheets commonly occupy shear zones that appear to have formed under highly ductile conditions, as evidenced by deformed nodules along the dike margins (Fig. 9). Chemical analyses (Table 1) establish that the host granite and the dikes have the same composition, and geochronology (presented in a later section) demonstrates a statistically identical age for the two. These results document that vein and nodule formation took place *during* the magmatic evolution of the leucogranite system, and the formation of both sets of veins and nodules is constrained to lie between emplacement of the granite pluton and late dikes such as those shown in Fig. 9.

The typical internal structure and composition of the veins and nodules is shown in a photomicrograph (Fig. 10) of rectangle 1–2 of Fig. 4. Within these features, sillimanite is commonly, but not invariably, concentrated towards the center of the vein or nodule and is surrounded by an envelope of quartz that is distinctly clearer and more

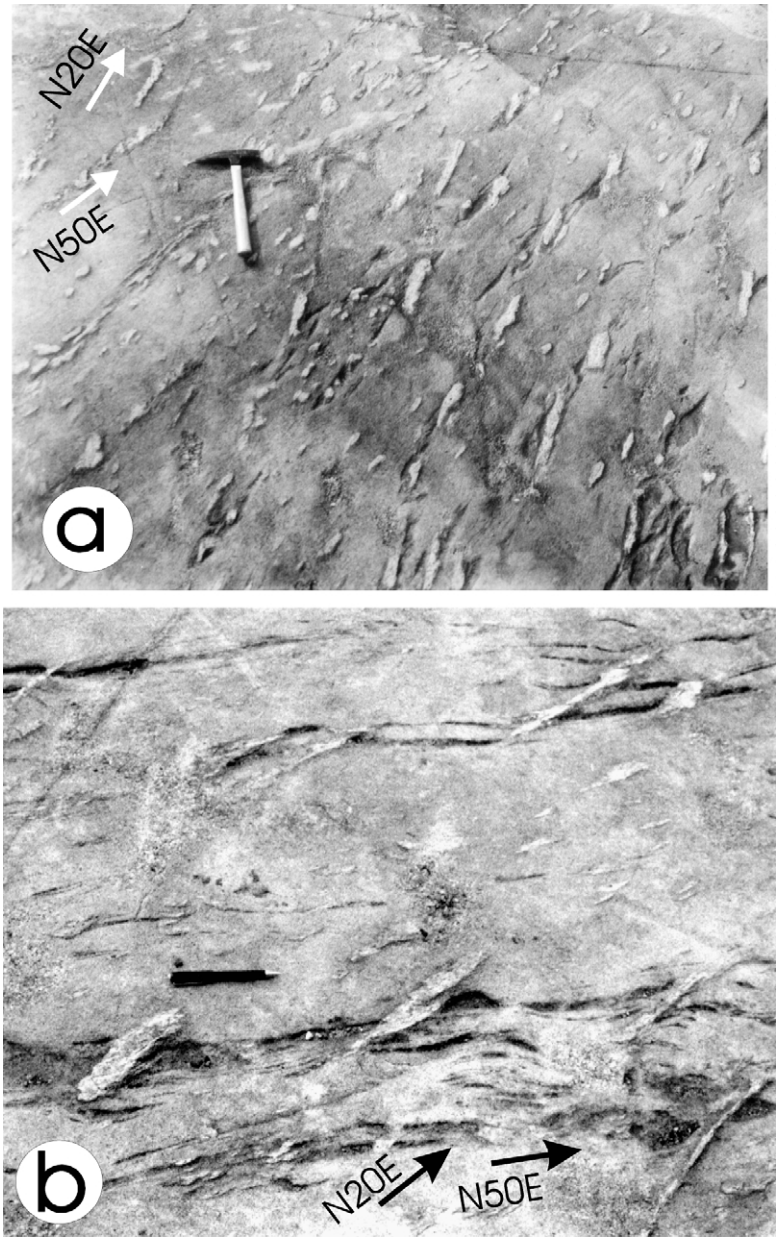

Fig. 5. Examples of nodule features and crosscutting relationships. Arrows give orientations. (a) Blocky and raggedly terminated N20E nodules crosscut dark calcsilicate schleiren in the Lyonsdale Falls leucogranite. Towards the center of the figure four N20E nodules define an aligned train that is interpreted as a disrupted vein. Smaller N50E nodules are arranged subparallel to, and crosscut, the schleiren. Hammer = 45 cm. (b) Close-up of N20E veinlets and nodules crosscutting dark calcsilicate schleiren. In several cases the veinlets occupy sinistral shear zones and appear to have an en échelon configuration. Pencil = 15 cm.

pristine than that of the host leucogranite. Small quantities of magnetite commonly accompany the quartz and sillimanite. McLelland et al. (2002) have discussed the geochemical evolution of these features. The zoned configuration of sillimanite and quartz is consistent with sequential growth from high temperature hydrothermal solutions moving through fracture systems.

The leucogranite itself is a pink, medium- to fine-grained, equigranular rock with aplitic texture and contains few dark minerals other than magnetite. A typical photomicrograph (Fig. 11) shows blocky, randomly oriented microcline–perthite grains, some of which preserve rectangular terminations indicative of a magmatic origin. Quartz grains are irregular in outline and some appear to embay the feldspars. The rock lacks any significant grain shape fabric due to deformation, nor is there any textural evidence, e.g. 120° contacts, of post-deformational annealing. This stands in marked contrast to the vast majority of quartzofeldspathic rocks in the Adirondack Mts. that exhibit pronounced deformational fabrics (McLelland, 1984) even when these units have experienced elevated metamorphic temperatures of 700–800°C. In such cases, individual grains may be

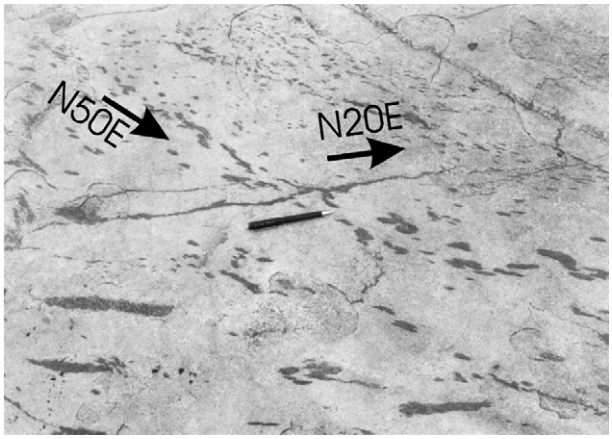

Fig. 6. In the center of the photograph an intact N20E (see arrows) vein crosscuts an aligned train of N50E (see arrows) nodules that represents a boudinaged early vein. The absence of deformation in the N20E vein demonstrates its later emplacement. Pencil = 15 cm.

annealed, but fabrics such as quartz ribbons and feldspar tails remain preserved. The absence of such fabrics in the rocks under investigation here suggests that they did not experience the pronounced ductile, subsolidus strain that is common in other Adirondack lithologies and that the textures seen in Fig. 11 are largely of igneous origin. This is further supported by geochronology discussed in a later section, which is consistent with a late- to post-tectonic origin for the pluton. If this is the case, then the deformation resulting in vein formation and disruption (e.g. Fig. 9) must be due to flow at magmatic or barely submagmatic temperatures. This possibility will be discussed in a later section.

Miller and Paterson (1994), Paterson and Tobisch (1994) and Paterson et al. (1989) describe deformation in syntectonic plutons as either: (1) magmatic (liquid dominated), (2) submagmatic (crystal mush capable of deforming by slip between crystals and migration of the melt fraction), or (3) solid state (insufficient melt to prevent crystal plastic deformation of crystals). They stipulate that magmatic deformation is difficult to discern, but that numerous features may define submagmatic flow. We note the presence of some of these in the leucogranite study area (schlieren layering, ductile shear zones and dikes perpendicular to magmatic foliation) but also note the paucity of others, such as *S–C* structure and pervasive magmatic foliation and lineation. One contributing factor to the general lack of magmatic foliations may be the absence of fabric forming minerals, such as amphiboles or micas. For the Mt. Stuart batholith, Miller and Paterson (1994) noted that it is in the pluton carapace that submagmatic features are best seen, similar to our observations in the leucogranite. Several lines of evidence, from experimental to direct measurements of natural lavas, suggest that submagmatic deformation may occur between melt contents of 20 and 50%. Thus, although we cannot identify the melt fraction in the leucogranite, we surmise that it was at least 30% as there are no localities at which solid-state crystal plastic deformation textures are observed. In addition, materials lying within the ductile regime can undergo fracture at sufficiently rapid rates of strain, including those associated with resurgent magma pulses (Fournier, 1999).

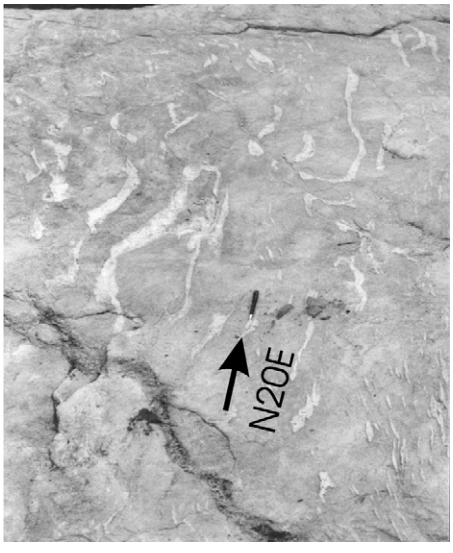

Fig. 7. Disrupted N20E (see arrow) veins exhibiting irregular and disharmonic folding. A swarm of small nodules can be seen in the lower right hand corner and a relatively undeformed NW-trending pegmatite dike crosses the lower portion of the figure. Pencil = 15 cm.

3. Age of the leucogranite

The leucogranite yielded a sparse population of rusty colored zircon grains with lengths in the 100–400 micron range and length to width ratios averaging 3:1 (Fig. 12a–d). Pyramidal terminations are common but many terminations are rounded. Most grains appear fractured and altered, but enough fresh specimens were available to permit single grain analysis by thermal ionization mass spectrometry (TIMS). Analytical details are presented in Appendix A. The majority of grains contain cores (Fig. 12d) surrounded by mantles of varying thickness but commonly accounting for ~50% of the grain volume. Many of these mantles exhibit oscillatory zoning characteristic of growth in magma (Fig. 12a). Several of these grains were strongly air abraded and the cores dated. Representative results are given in Table 2 and establish that the cores fall into a range of ca. 1180–1130 Ma, which corresponds to the voluminous anorthosite–mangerite–charnockite–granite (AMCG) suite of the Adirondacks (McLelland et al., 1996). A non-abraded, cored grain yields an age of ca. 1120 Ma that represents a mixed age between the core and mantle (Table 2).

A small population of non-cored, well terminated, relatively clear, igneous looking grains and fragments were hand picked, air abraded for brief intervals, and analyzed by TIMS techniques (see Appendix A). The results for six of

Fig. 8. Late quartz–sillimanite veins wander in open folds across an outcrop surface containing numerous nodules representing disrupted earlier veins. Note that in several places the veins display incipient disruption into nodules. Arrow gives orientation. Pencil = 15 cm.

Table 1
Chemical composition of Lyonsdale Falls leucogranite

	PL-3-98	AFEQ	AF-95
Oxide			
SiO_2	76.71	76.68	76.03
TiO_2	0.22	0.26	0.11
Al_2O_3	12.22	12.47	12.59
Fe_2O_3	1.22	1.07	0.73
MnO	0.11	0.08	0.09
MgO	0.17	0.12	0.15
CaO	0.46	0.41	0.3
Na_2O	2.46	2.31	2.37
K_2O	5.09	5.52	5.44
P_2O_5	0.23	0.11	0.01
LOI	0.23	0.47	0.45
Total	99.12	99.5	98.27
Rb	228	232	223
Sr	53	57	121
Y	75	59	83
Zr	314	315	325
Nb	15	20	12
Ba	180	194	266

these are given in Table 2 and plotted in Fig. 13. The best of these was a relatively clear grain, that exhibited no core, had sharp double terminations, and showed traces of fine scale zoning — all of which indicate an origin by growth in magma This grain is 100% concordant at 1031 ± 7.8 Ma, and this must include the crystallization age of the magma. Together with the remaining five prismatic fragments, these points define an upper intercept on concordia of 1035.1 ± 3.8 Ma. This age is taken to represent the time of emplacement of the leucogranite. The cored grains (Table 2) fall well to the right of concordia and were not plotted due to scale.

Pegmatites such as that coring the composite dike in Fig. 9 belong to a NW striking set of dikes that represent the latest magmatic features in the area. They crosscut all exposures of leucogranite and clearly truncate quartz–sillimanite veins and nodules. A meter-wide member of this family of pegmatites has been dated by TIMS methods (McLelland et al., 2001) and yields an upper intercept age of 1034 ± 10 Ma, which is not statistically different from the age of the leucogranite (Fig. 13). We conclude that the crosscutting pegmatites represent the terminal magmatic phase of a leucogranite pluton and that the formation of the quartz–sillimanite veins and nodules must fall into a geologically brief time interval between these two events.

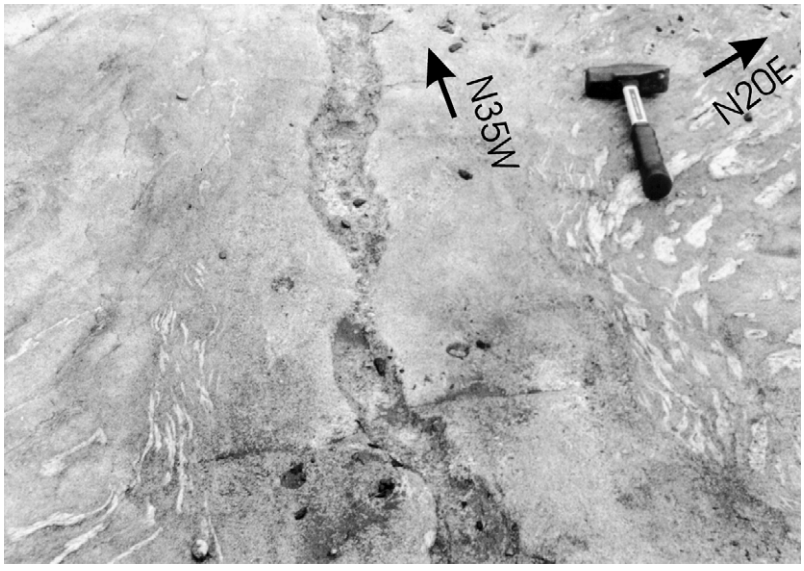

Fig. 9. In the center of the picture a composite dike of nodule-free leucogranite and pegmatite crosscuts nodular leucogranite of the same composition. The dike fills a NW-trending sinistral shear zone that has resulted in pronounced ductile deformation of N20E nodules along its margins. Orientation given by arrows. Hammer = 45 cm.

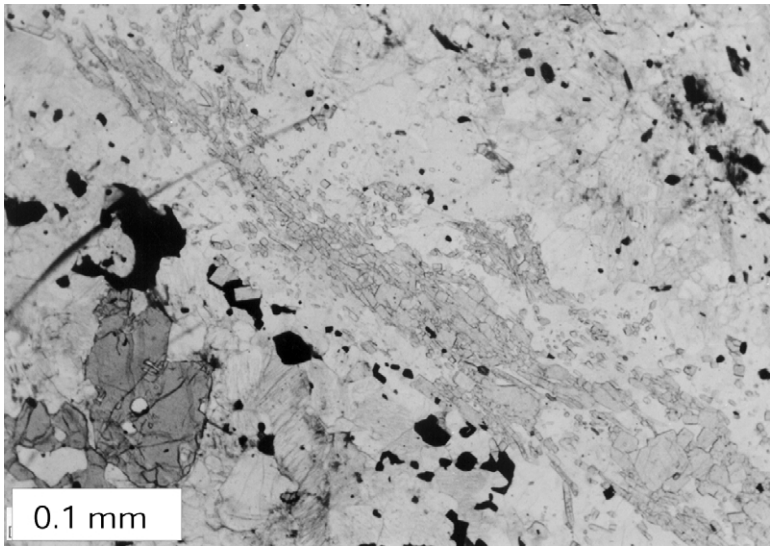

Fig. 10. Photomicrograph of typical quartz–sillimanite nodule showing prismatic needles of sillimanite concentrated at the center and enveloped by clear vein quartz. Groundmass quartz and feldspar appear as somewhat murky. Magnetite occurs along the lower margin of the nodule. A large garnet is present beneath the magnetite.

4. Anisotropy of magnetic susceptibility

The anisotropy of magnetic susceptibility (AMS) is a measurement that, among other applications, has been widely used for detecting fabrics in apparently undeformed igneous rocks (e.g. Ellwood and Whitney, 1980; Hrouda, 1982; Borradaile, 1988; McNulty et al., 2000). AMS is defined as a lack of parallelism between applied and induced magnetic fields and is caused by either shape-preferred orientation of magnetite or crystallographic-preferred orientation of hematite. Paramagnetic phases, such as hornblende, chlorite or biotite, may also contribute to the AMS signal of a rock but these phases are absent in the leucogranite discussed in this paper. Because AMS is a second order tensor, similar to stress or strain, it may be adequately represented by an ellipsoid with maximum (K_1), intermediate (K_2) and minimum (K_3) principal susceptibilities as the axes. Numerous studies have illustrated the parallelism between the AMS axes and mesoscopic foliation and lineation in granitoids (e.g. Cruden and Launeau, 1994; Rochette et al., 1994; Benn et al., 1997). Thus, in the absence of mesoscopic foliation and lineation, AMS may be used to discern the orientations of the flow plane and flow direction in igneous rocks. The orientation of AMS maxima is a proxy for the direction of magmatic flow whereas the plane defined by the K_1 and K_2 directions (perpendicular to

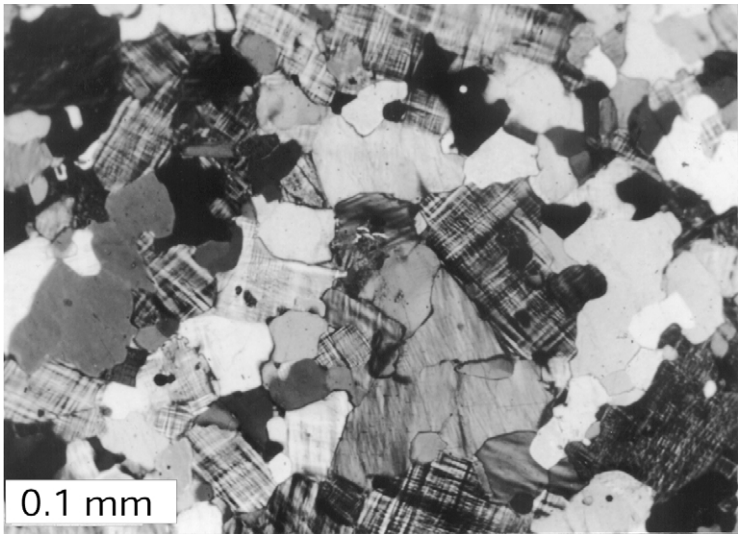

Fig. 11. Photomicrograph of typical leucogranite from Lyonsdale. Randomly oriented, rectangular grains of microcline–perthite exhibit many angular grain boundaries close to 90°. Irregular, light colored regions consist of quartz some of which appears to embay the feldspar grains. The texture is interpreted as igneous and shows no tectonic grain shape fabric.

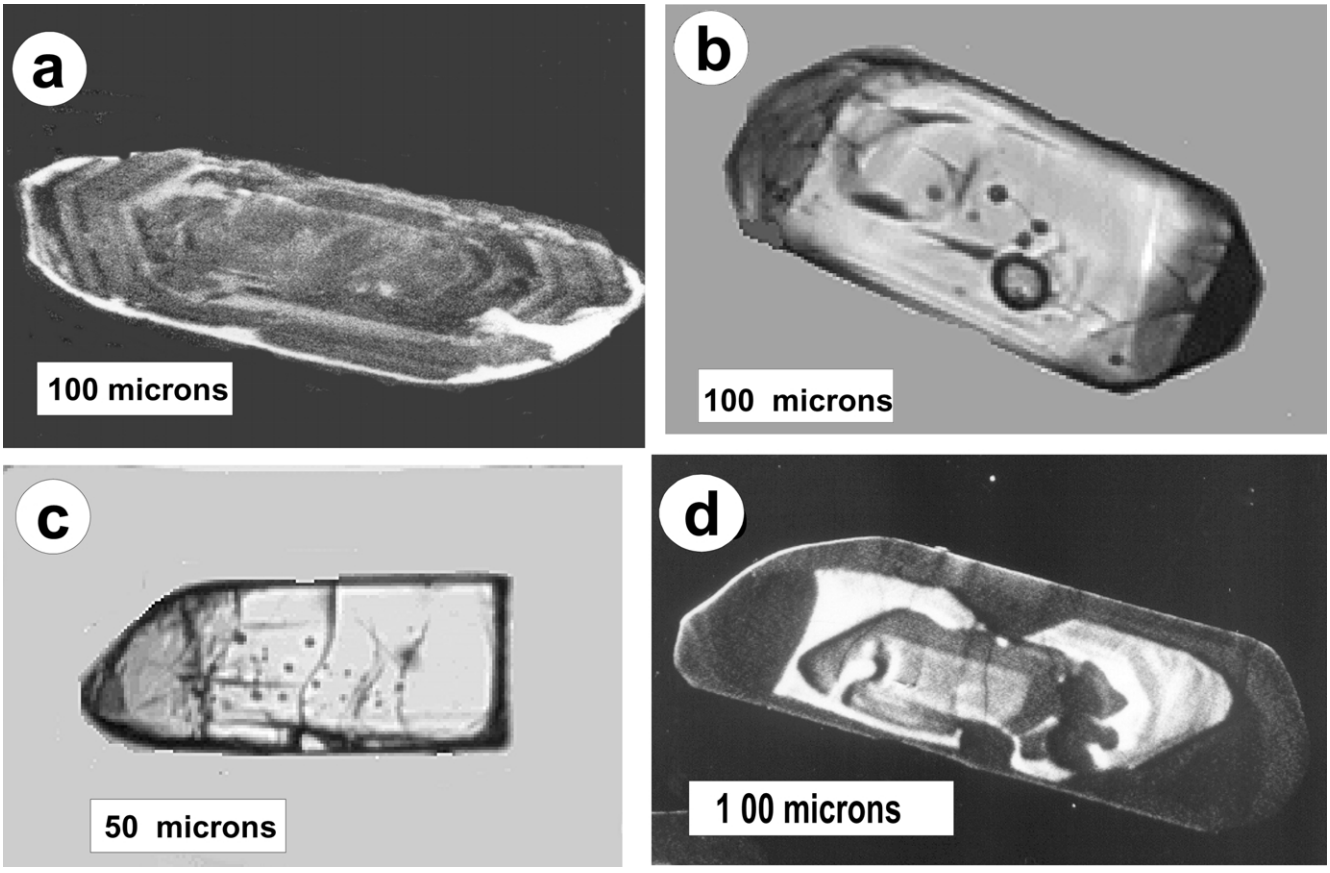

Fig. 12. Images of zircons from the Lyonsdale Falls leucogranite. (a) SEM image of an elongate, core-free grain with pyramidal terminations and pronounced oscillatory zoning. (b) Transmitted light image of a core-free, doubly-terminated zircon. Apparent differences between the bright, rectangular center and the dark terminations are due to focusing and refraction. (c) Transmitted light image of a pyramidally terminated, non-cored prismatic fragment. (d) SEM image of a complexly cored grain.

the K_3 direction) is taken as representative of the flow plane. The orientations of these axes as well as the shape of the ellipsoid and its ellipticity, may be represented in manners similar to strain, with which AMS has been correlated in ductilely deformed rocks.

Sixty-two (62) samples of leucogranite were collected at the exposures described above. Samples were oriented in the field and their AMS was measured with a KLY-2 Kappabridge. The orientations of maximum principal susceptibility are tightly clustered around the horizontal direction N49E and the maximum-intermediate plane strikes N49E and dips 57 to the NW (Fig. 14a). The shapes of susceptibility ellipsoids are shown in Fig. 14b and illustrate the oblate to highly oblate nature of most of the fabric measurements. It is apparent that the further from the origin a point lies (more anisotropic), the closer it is to the $K2/K3$ axis. This indicates that the shape of the AMS ellipsoid varies with it's intensity so that the greater the anisotropy, the more highly oblate the ellipsoid. The ellipticity of the susceptibility tensor is illustrated as a histogram of percent anisotropy (Fig. 14c), calculated as $\{(K1 - K3)/\text{average}\} \times 100$. As indicated by Fig. 14c, many of the samples of leucogranite are very highly anisotropic with numerous anisotropies lying above 50% and an average of 42%. For comparison, similar intrusive rocks typically display anisotropy less than 20% (McNulty et al., 2000). The results outlined briefly above are strongly indicative of very highly deformed rocks that experienced sub-horizontal flow in a direction approximately N50E with a flow plane inclined moderately to the NW.

5. Structural model

We propose a model that incorporates deformation and fracturing of ductile leucogranite and its incompletely crystallized magma (cf. Nicolas and Jackson, 1982; Nicolas, 1986; Bottinga, 1994; Rubin, 1998; Fournier, 1999; Gillis and Roberts, 1999) thereby accounting for quartz–sillimanite vein formation at the margins of a pluton in a fashion consistent with observations and their implications. These include: (1) quartz–sillimanite veins lie in two dominant directions (N50E, approximately parallel to the pluton contact, and N20E); (2) the N50E veins are more disrupted and are crosscut by the N20E veins; (3) veins were formed by hydrothermal alteration in the carapace of

Table 2
Zircon isotopic data of Lyonsdale leucogranite (mg — milligram, μg — microgram, pg — picogram, Pb-c — common lead, wg — whole grain, prm — prism, nc — not cored, cl — clear, aa — air abraded, r — rusty, fracd — fractured, db term — doubly terminated)

Grain	Description	Mass (μg)	U (ppm)	Pb (ppm)	Pb-c (pg)	$^{206}Pb/^{204}Pb$	$^{206}Pb/^{238}U$	± 206/238[a]	$^{207}Pb/^{235}U$	± 207/235[a]	$^{207}Pb/^{206}Pb$	± 207/206[a]	Age $^{206}Pb/^{238}U$	Age $^{207}Pb/^{235}U$	Age $^{207}Pb/^{206}Pb$[c]	± Age 207/206	Percent concord.[b]
LB-5	fracd prm,cl,nc	1	3672	669	77	464	0.156801	1.03	1.60152	1.04	0.075256	0.14	929	973	1044.8	5.7	89
LB-6	prm, term, aa, nc	1	7192	1252	76	932	0.162203	0.94	1.65211	0.98	0.074919	0.16	957.8	991.4	1038.9	4.9	92
LB-7	fracd prm, r, nc	1	3964	600	15	2301	0.143341	0.96	1.46263	0.98	0.074203	0.12	861.4	915.1	1047.1	2.5	82
LB-8	prm, r, nc	1	1456	139	14	894	0.138632	1.41	1.41453	1.42	0.074002	0.16	836.9	895.1	1041.5	3.2	80
LB-9	wg,nc,db term,aa	1	1259	221	5.5	2413	0.173692	1.32	1.76311	1.41	0.073621	0.38	1032.4	1032.1	1031	7.8	100
LB-10	prm,dbl term,cl,nc	1	5006	713	26	1539	0.131851	1.04	1.34802	1.12	0.073513	0.13	799.3	862.3	1049.1	2.6	76
Not plotted																	
LB-1	cored	1	2899	558	14	2175	0.174231	0.53	1.84806	0.54	0.076929	0.08	1035.4	1062.7	1119.4	1.6	92
LB-2	aa to core	1	67	21	5.2	171	0.200978	7.42	2.19722	8.23	0.079291	3.38	1180.6	1180.2	1179.4	3.4	100
LB-3	cored, aa	1	456	106	9.7	533	0.183006	1.32	1.95681	1.48	0.077551	0.63	1083.4	1100.8	1135.4	13	95

[a] Errors reported at 2-sigma percent.
[b] Percent concordancy is the degree of concordancy, in percent, between the $^{207}Pb/^{206}Pb$ and $^{206}Pb/^{238}U$ ages.
[c] Errors reported at 2-sigma in Ma.

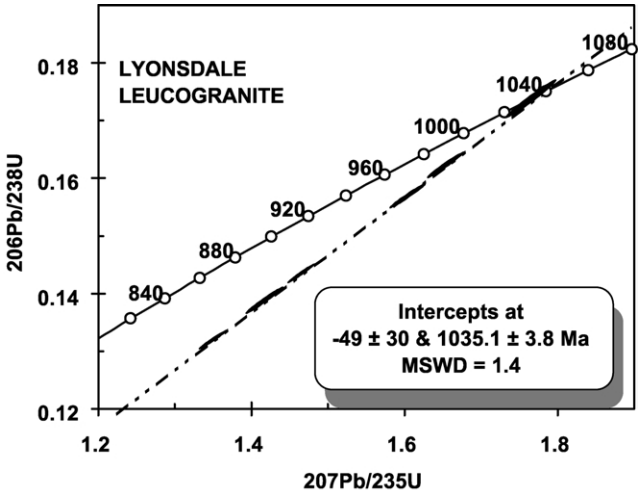

Fig. 13. Concordia diagram of six single zircon grains from the Lyonsdale Falls leucogranite. The upper intercept and concordant point are interpreted as representing the time of emplacement of the leucogranite. Error ellipses are plotted at 2-sigma.

the cooling pluton; (4) magma was still present during the formation of the veins (Fig. 9); and (5) AMS data suggest subhorizontal flow during deformation of the pluton carapace.

The model begins with the intrusion of the leucogranite into surrounding calc–silicate country rock (Fig. 15a). The abundant schlieren in the leucogranite at Lyonsdale Falls strongly suggest that this locality is situated close to the pluton margin and that strong deformation has aligned the schlieren parallel to this margin. This alignment could have been produced either by magmatic flow parallel to the margin or flattening against the margin as the pluton inflated. It is difficult to tell if deformation of the partially molten leucogranite was caused by tectonic stress or stresses generated within the pluton (see Paterson et al. (1998) for a general review). We note the parallelism between magmatic foliation and the pluton margins and suggest that shearing along the margins of the pluton was constrained by margin orientation and could have been caused either by internal magmatic processes or by external tectonic stress. Whereas complex patterns of flow may exist in an active, cooling pluton, both as a result of tectonic or plutonic processes (Paterson et al., 1998), the area studied here is sufficiently small and close to the pluton margin that most of these complexities do not affect our interpretations. The model in Fig. 14 is based on a NNE-oriented σ_1 and this could represent either a regionally imposed tectonic stress or simply a local stress orientation generated by magmatic processes. Considering that the AMS foliation, mesoscopic foliation, schlieren and the pluton margin are all inclined at approximately 50°, it is most likely that the fractures were not originally vertical. If the fluid pressure in the partially molten magma increased, low differential stress would be capable of initiating mode I fractures (Fournier, 1999), which would have localized fluids and lead to the formation

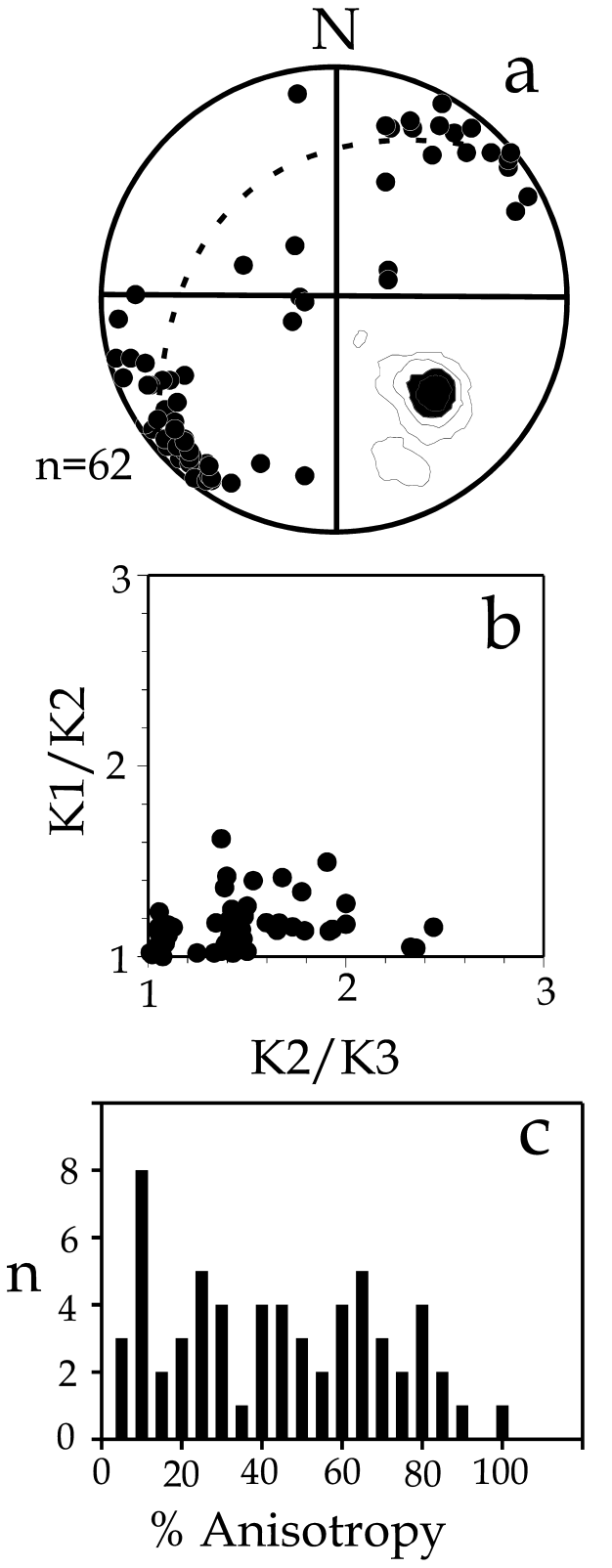

Fig. 14. AMS data. (a) Lower hemisphere equal area stereographic projection of AMS maxima (K_1; solid circles), minima (K_3; contours; 5, 10, 15, 20, 25% per 1% area) and $K_1 - K_2$ great circle (dashed). (b) Flinn diagram showing shapes of AMS ellipsoids. (c) Histogram of percent anisotropy ({[max − min]/avg} × 100)

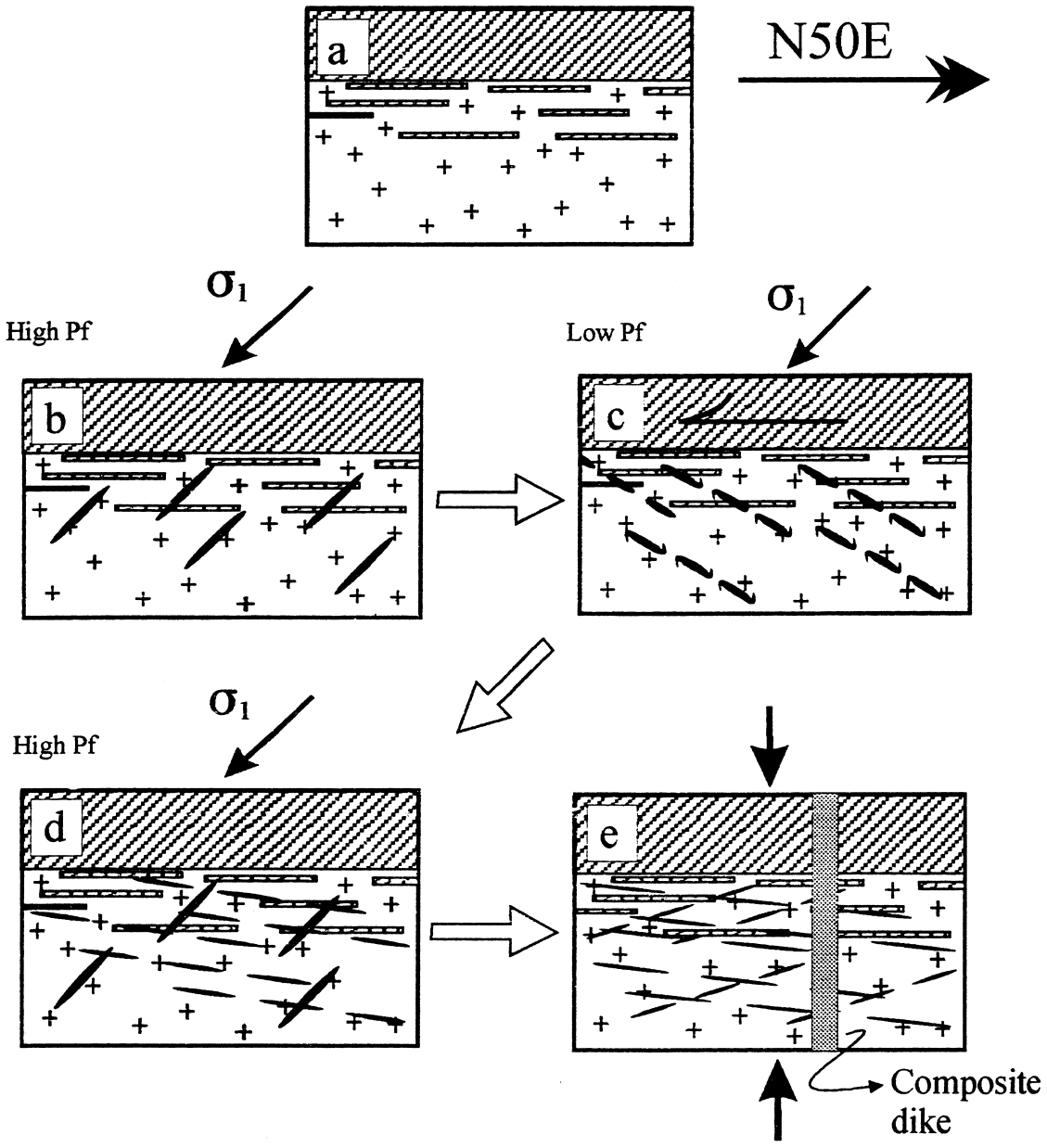

Fig. 15. Structural model of development of quartz–sillimanite veins at Lyonsdale Falls (see text for full explanation). (a) Intrusion of leucogranite into calcsilicate country rock; schlieren are aligned either by magmatic flow or by flattening of the pluton against the N50E contact. (b) Initial formation of veins within the pluton carapace. (c) Deformation of veins by sinistral shear along pluton contact. Veins rotate counterclockwise and extend by boudinage. (d) A second episode of vein formation. (e) Deformation of all veins by pluton inflation and flattening of the ductile carapace against the contact. Late composite dikes and pegmatites form at this time approximately parallel to direction of shortening.

of vein-hosted quartz–sillimanite veins. This mechanism is consistent with the petrologic and geochemical evidence for large volumes of water during vein formation (McLelland et al., 2002). Initial vein orientations would have been sub-vertical and NNE, parallel to the maximum principal compression (Fig. 15b). Consequent upon the decrease of fluid pressure due to fracture-induced dilatancy, fracturing would have been suppressed and the ductile carapace of the pluton would have localized sinistral shear at a low strain rate (Fig. 15c). With progressive shear, veins would become rotated in a counterclockwise sense and would have experienced shortening followed by extension. Observations of both buckled and boudinaged veins are consistent with this hypothesis (Fig. 7). It is not possible to recover the precise strain fields that caused vein disruption and either sub- or super-simple shear could have resulted. Under conditions of sub-simple shear, back rotation of veins might have occurred and, thus, although our model envisions only counterclockwise rotations, other patterns of movement could also have resulted in alignment of

disrupted veins. As veins rotated progressively toward the shear zone boundary, they would have experienced increasing amounts of extension and extreme flattening and boudinage would have occurred. We note that objects with large aspect ratios, such as the schlieren, rotate very slowly as they approach parallelism with the shear zone boundary, in essence pinning them in this orientation (Jeffrey, 1922; Ramsay, 1967; Ramsay and Huber, 1983). Objects with smaller aspect ratios continue to rotate resulting in crude parallelism between boudinaged veins and schlieren. If fluid pressures increased again, a new episode of fracturing would have been initiated with new veins oriented NNE (Fig. 15d). This process could have taken place repeatedly, resulting in numerous generations of veins, all of which would have progressively rotated towards parallelism with the pluton margin.

We note that nearly all veins are disrupted and boudinaged thus suggesting the existence of very late stage pluton inflation. A nearly irrotational shortening at high angles to the pluton contact would have served to rotate all veins towards parallelism with the contact and would also cause disruption of younger veins with NNE strikes (Fig. 15e). Numerous pegmatites and composite dikes (Fig. 9) are present in the exposures in the Moose River bed and strike nearly perpendicular to the pluton contact (~N40W). These dikes are among the youngest features present in these exposures (Fig. 9) and truncate all veins. The timing of intrusion and orientation of these dikes is consistent with the proposed late-stage pluton inflation (Fig. 15e). We note that even the young composite dikes have localized sinistral shear. Such observations require either a rotation of the maximum principal compression to a nearly EW orientation, appropriate for sinistral shear on NW striking dikes, or some intrusion-related displacements resulting in deformation of the dike margins. Our observations are currently insufficient to differentiate between these two options.

An alternate hypothesis for the origin of fracturing within the pluton carapace relies on changes in strain rate to cause fracturing (Fournier, 1999). Bottinga (1994) noted that under rapid strain rates, a crystal mush can undergo fracture. The orientations of veins produced by rapid sinistral shear along the pluton contact would be close to those illustrated in Fig. 15. Such a model would have veins forming during episodes of rapid sinistral shear. During times of slower strain rates, sinistral shear along the pluton contact would rotate and deform veins as described above and illustrated in Fig. 15c. Additional rapid strain could cause new fractures, similar to the situation illustrated in Fig. 15d and final vein rotation and deformation would take place through pluton inflation and flattening against the pluton contact, as shown in Fig. 15e. We favor the first model over the second largely because of the abundant evidence of fluid and the strong similarity between our ideas regarding fluid pressure and those documented in Fournier (1999).

6. Conclusions

The results summarized in previous sections demonstrate that the quartz–sillimanite veins and nodules formed within the host leucogranite during the interval between its emplacement (1035.1 ± 3.8 Ma) and that of closely related pegmatite dikes (1034 ± 10 Ma). Throughout this interval leucogranitic magma remained present and resulted in resurgent intrusions documented by late dikes that crosscut the vein–nodule complex (Fig. 9). The veins and nodules formed within fractures that crosscut both the leucogranite and calcsilicate schleiren within it and cannot be the result of material incorporated into the pluton. As discussed by McLelland et al. (2002), the quartz–sillimanite mineralogy of the veins and nodules is the result of leaching of cations from wall rock feldspars in the leucogranite by acidic magmatic hydrothermal solutions.

Several demonstrable periods of vein and nodule formation are evident, and these are characterized by crosscutting relationships with one another and with host rocks. Inspection of the nodules reveals that most, if not all, are the result of boudinage and boudin separation along extensional trajectories commonly marked by nodule trains. This disruption must have taken place under extremely ductile and high temperature conditions, because the intervening granite shows little, if any, evidence of grain shape fabric that would be expected to develop during ordinary solid state strain. This ductility is manifested by the pronounced deformation of nodules at the dike margin in Fig. 9 and by the absence of any tectonic grain shape fabric in the host granite. Indeed the granite at the dike margin exhibits the same equigranular, igneous texture as that shown in Fig. 11 and characterizes most of the Lyonsdale Falls leucogranite.

The foregoing constraints are best accounted for if the fractures in which the veins and nodules formed were the result of sequential strain occurring within the largely solidified carapace of an intruding body of leucogranite. The flow directions within the leucogranite have been studied with AMS and results indicate that magmatic flow was subhorizontal in a direction N49E and that the flow plane was inclined moderately to the NW. These data, together with the subvertical orientations of the veins, suggest that vein formation occurred in a stress system with the maximum principal stress subhorizontal and two models for vein formation within a deforming crystal mush can be proposed. One model incorporates high fluid pressures to initiate fractures (Hibbard, 1987) and deformation by sinistral shear during times of low fluid pressure. The other model resorts to changes in strain rate to initiate fractures (Bottinga, 1994) but retains sinistral shear as a mechanism to disrupt the veins. Final vein disruption is viewed as resulting from flattening of the carapace against the pluton contact, perhaps in association with pluton inflation. Resurgent pulses of magma would initially give rise to renewed fracturing, and this would be followed by heating and increased ductility in the carapace. In this

regard the carapace can be envisaged as an evolving conductive boundary zone of the sort described by Gillis and Roberts (1999) for the Troodos Ophiolite. Within such zones oscillatory pressure due to magma surge, fluid evolution, and synemplacement strain will all combine to result in a variety of rotational strains that are capable of producing the vein–nodule complex described above.

The age of the Lyonsdale Falls leucogranite is among the youngest igneous rock dates recorded within the Adirondacks (McLelland et al., 2001) and closely approximates the ca. 1050 ± 10 Ma age of LMG (McLelland et al., 2002). The texture, mineralogy and chemical composition of the leucogranite is also very similar to that of LMG. Furthermore, quartz–sillimanite veins and nodules are known from other occurrences of LMG across the Adirondacks and are rarely encountered in any other unit. Finally, it is significant that both LMG and the Lyonsdale Falls leucogranite contain very few dark minerals other than magnetite, a property that is characteristic of these units only. At several localities within the Adirondacks, magnetite concentrations within, or associated with, LMG have been developed into historically significant magnetite mines (e.g. Lyon Mt., Mineville, Moriah), including deposits consisting of iron-oxide, sillimanite, and garnet (e.g. Star Lake). At Lyonsdale Falls hydrothermal veins of magnetite and sillimanite exist at several localities within the leucogranite and several pegmatites contain concentrations of magnetite. These unusual similarities strongly suggest that the Lyonsdale Falls leucogranite and its vein–nodule complex are very late representatives of LMG. In northern New Jersey similar granites occurring at Mt. Adam and Mt. Eve have been dated at 1020 ± 4 Ma (Drake et al., 1991). These granites are undeformed, and like the Lyonsdale Granite and LMG set a lower time limit for termination of the Ottawan Orogeny.

Acknowledgements

McLelland gratefully acknowledges NSF research grant EAR- 98-28947. Both McLelland and Goldstein gratefully acknowledge generous support from the Colgate Research Council. We thank Pat Bickford and Scott Samson for making available the geochronological facilities at Syracuse University. Chapin Brackett and Will Willis were of great help during the summers of 1995 and 1996. Throughout this investigation we received much helpful guidance from Ron Vernon, Dugald Carmichael, Peter Nabelek, Mike Williams, Sheila Seaman, Lawford Anderson, and Jean Morrison. We thank Keith Klepeis, Bob Miller, and Colin Shaw who provided thoughtful and very helpful reviews. Mike Williams' editorial advice was most helpful in improving the manuscript.

Appendix A

Single grain determinations were performed at the Isotope Geochemistry Lab of Syracuse University Geology Department. Samples were crushed and minerals separated using standard equipment and methods. Desirable grains were handpicked and chemically processed by standard techniques (Krogh, 1973; Parrish, 1987) and were spiked with either a mixed $^{205}Pb/^{235}U$ tracer or a mixed $^{208}Pb/^{235}U$ tracer. Air abraded fractions were prepared using the techniques of Krogh (1982) Four total procedural blanks were run in parallel with samples. Blanks were spiked after column chemistry before drying down with approximately 1 ng of Pb as SRM983. U and Pb wre chemically separated using exchange minicolumns following the proceedure of Krogh (1973). Samples were loaded on outgassed, zone-refined Re filaments using silica gel and phosphoric acid. Blanks ranged from 3 to 10 pg total Pb. Uranium blanks were approximately 3 pg. Samples were run on a VG Sector multi-collector mass spectrometer fitted with a Daly photomultiplier in the axial position. The in-run fractionation correction using the Daly in multicollector mode was 0.18%/amu for all ratios. No correction was made for in-run fractionation of U. Data reduction was completed using decay constants $^{238}U = 0.155125 \times 10^{-09}$ and $^{235}U = 0.9845 \times 10^{-09}$ of Steiger and Jaeger (1977), and the software by Ludwig (1983, 1992). The Pb-blank value used to reduce data for any fraction was that for the blank run in parallel with that dissolution. The initial common Pb composition used to reduce data for any given fraction was the composition of lead calculated using the Stacey and Kramers (1975) lead evolution model at the approximated $^{207}Pb/^{206}Pb$ age of that fraction. Errors for radiogenic ratios are reported at ± 2((and for Pb207/Pb206 age as ± 2(Ma.

References

Benn, K., Horne, R.J., Kontak, D.J., Pignotta, G.S., Evans, N.G., 1997. Syn-Acadian emplacement model for the South Mountain batholith, Meguma terrane, Nova Scotia: magnetic fabric and structural analysis. Geological Society of America Bulletin 109, 1279–1293.

Borradaile, G., 1988. Magnetic susceptibility, petrofabrics and strain. Tectonophysics 156, 1–20.

Bottinga, Y., 1994. Rheology and rupture of homogeneous silicate liquids at magmatic temperatures. Journal of Geophysical Research 99, 9415–9422.

Buddington, A.F., Leonard, B., 1962. Regional geology of the St. Lawrence county magnetite district, northwest Adirondacks, New York. U.S. Geological Survey Professional Paper 376, 145 p.

Cruden, A.R., Launeau, P., 1994. Structure, magnetic fabric and emplacement of the Archean Label stock, SW Abitibi greenstone belt. Journal of Structural Geology 16, 677–691.

Drake, A.A., Aleinikoff, J.N., Volkert, R.A., 1991. The Mount Eve Granite (Middle Proterozoic) of northern New Jersey and southeastern New York. U.S. Geol. Surv. Bull 1952, C1–C10.

Ellwood, B.B., Whitney, J.A., 1980. Magnetic fabric of the Elberton Granite, northeast Georgia. Journal of Geophysical Research 85, 1481–1486.

Fournier, R.O., 1999. Hydrothermal processes related to movement of fluiod from plastic into brittle rock in the magmatic–epithermal environment. Economic Geology 94, 1193–1212.

Gillis, K.M., Roberts, K.D., 1999. Cracking at the magma–hydrothermal transition: evidence from the Troodos Ophiolite, Cyprus. Earth and Planetary Science Letters 169, 227–244.

Hibbard, M.J., 1987. Deformation of incompletely crystallized magma systems: Granitic gneisses and their tectonic implications. Journal of Geology 95, 543–561.

Hrouda, F., 1982. Magnetic anisotropy of rocks and its application in geology and geophysics. Geophysical Surveys 5, 37–82.

Jeffrey, G.B., 1922. On the motion of ellipsoidal particles immersed in a viscous fluid. Proceeds of the Royal Society of London, Series A 102, 161–179.

Kerrick, D.M., 1988. Al_2SiO_5-bearing segregations in the Leopontine Alps, Switzerland: aluminum mobility in metapelites. Geology 16, 636–640.

Krogh, T.E., 1973. A low-contamination method for hydrothermal decomposition of zircon and extraction of U and Pb for isotopic age determinations. Geochimica Cosmochimica Acta 37, 485–494.

Krogh, T.E., 1982. Improved accuracy of U–Pb zircon ages by creation of more concordant systems using an air abrasion technique. Geochimica Cosmochimica Acta 46, 637–649.

Losert, J., 1968. On the genesis of nodular sillimanitic rocks. XXIII International Geological Congress 4, 109–122.

Ludwig, K.R., 1983. Plotting and regression programs for isotope geochemists, for use with HP-86/87 microcomputers. U.S. Geological Survey Open File Report 83-849, 94 p.

Ludwig, K.R., 1992. ISOPLOT: a plotting and regression program for radiogenic isotopic data. Version 2.57. U.S. Geological Survey Open File Report 91-455.

Markl, G., Schumacher, J.C., 1996. Spatial variations in temperature and composition of greisen-forming fluids: an example from the Variscan Triberg Granite Complex, Germany. Economic Geology 91, 576–589.

McLelland, J., 1984. Origin of ribbon lineation in quartzofeldspathic gneisses of the Adirondacks. In: Ramsey, J. (Ed.). Linear and Planar Fabrics In Tectonic Rocks. Journal of Structural Geology 6, pp. 147–167.

McLelland, J., Daly, J.S., McLelland, J.M., 1996. The Grenville Orogenic Cycle (ca 1350–1000 Ma): an Adirondack perspective. Tectonophysics 265, 1–28.

McLelland, J., Hamilton, M., Selleck, B., McLelland, J.M., Orrell, S., Walker, D., 2001. Zircon geochronology of the Ottawan Orogeny, Adirondack Highlands, New York. Precambrian Research 109, 39–72.

McLelland, J., Morrison, J., Selleck, B., Cunningham, B., Olsen, C., 2002. High temperature hydrothermal alteration of late- to post-tectonic Lyon Mt Granitic Gneiss, Adirondack Highlands, New York: origin of quartz–sillimanite nodules, quartz–albite facies, and associated low-Ti,Fe-oxide deposits of the Kiruna type. Journal of Metamorphic Geology (in press).

McNulty, B., Tobisch, O.T., Cruden, A., Gilder, S., 2000. Multistage emplacement of the Mount Givens pluton, central Sierra Nevada batholith, California. Geological Society of America Bulletin 112, 119–135.

Miller, R.B., Paterson, S.R., 1994. The transition from magmatic to high-temperature solid-state deformation: implications from the Mount Stuart batholith, Washington. Journal of Structural Geology 16, 853–865.

Nabeleck, P.I., 1997. Quartz–sillimanite leucosomes in high grade schists, Black Hills, South Dakota: A perspective on the mobility of aluminum in high grade metamorphic rocks. Geology 25, 995–998.

Nicolas, A.A., 1986. A melt extraction model based on structural studies in mantle peridotites. Journal of Petrology 27, 999–1022.

Nicolas, A.A., Jackson, M., 1982. High temperature dikes in peridotites: origin by hydraulic fracturing. Journal of Petrology 23, 568–582.

Parrish, R.R., 1987. An improved micro-capsule for zircon dissolution in U–Pb geochronology. Chemical Geology 66, 99–102.

Paterson, S.R., Tobisch, O.T., 1994. Rates of processes in magmatic arcs: implications for the timing and nature of pluton emplacement and wall-rock deformation. Journal of Structural Geology 14, 291–300.

Paterson, S.R., Vernon, R.H., Tobisch, O.T., 1989. A review of criteria for the identification of magmatic and tectonic foliations in granitoids. Journal of Structural Geology 11, 349–363.

Paterson, S.R., Fowler Jr, K.T., Schmidt, K.L., Yoshinobu, A.S., Yuan, E.S., Miller, R.B., 1998. Interpreting magmatic fabric patterns in plutons. Lithos 44, 53–82.

Postel, A.W., 1952. Geology of the Clinton County magnetite District, New York. U.S. Geological Survey Professional Paper 237, 88 p.

Ramsay, J.G., 1967. Folding and Fracturing of Rocks. McGraw-Hill Book Co, New York, 568 p.

Ramsay, J.G., Huber, M., 1983. The Techniques of Modern Structural Geology Vol. I: Strain Analysis. Academic Press, New York, 307 p.

Rivers, T., 1997. Lithotectonic elements of the Grenville Province: review and tectonic implications. Precambrian Research 86, 117–154.

Rochette, P., Scaillet, B., Guillot, S., LeFort, P., Pecher, A., 1994. Magnetic properties of the High Himalaya leucogranites: structural implications. Earth and Planetary Science Letters 126, 217–234.

Rubin, A.M., 1998. Dike ascent in partially molten rock. Journal of Geophysical Research 103, 20,901–20,919.

Stacey, J.S., Kramers, J.D., 1975. Approximation of terrestrial lead isotope evolution by a two-stage model. Earth and Planetary Science Letters 26, 207–221.

Steiger, R., Jaeger, E., 1977. Subcommission on geochronology: convention on the use of decay constants in geo- and cosmochronology. Earth and Planetary Science Letters 36, 359–362.

Vernon, R.H., 1979. Formation of late sillimanite by hydrogen metasomatism (base leaching) in some high grade gneisses. Lithos 12, 143–152.